

## Infrared-absorption and photoinduced-absorption spectroscopy of semiconducting $\text{YBa}_2\text{Cu}_3\text{A}\text{O}_{6+x}$ ( $A=16$ and $18$ ; $0 \leq x \leq 0.3$ )

H. J. Ye\* and R. P. McCall

*Department of Physics, The Ohio State University, Columbus, Ohio 43210-1106*

W. E. Farneth and E. M. McCarron III

*E. I. du Pont de Nemours and Co., Inc., Central Research and Development Department, Experimental Station, Wilmington, Delaware 19880-0356*

A. J. Epstein

*Department of Physics and Department of Chemistry, The Ohio State University, Columbus, Ohio 43210-1106*

(Received 31 July 1990)

We report the infrared (ir) absorption and photoinduced absorption (PA) spectra of semiconducting  $\text{YBa}_2\text{Cu}_3\text{A}\text{O}_{6+x}$  for  $A=16$  and  $18$  and for  $0 \leq x \leq 0.3$ . We observe ten ir absorption modes for  $x=0.3$  and report the first observation for all 11 allowed ir modes for  $x=0.0$ . The ir modes for  $x=0.0$  and  $x=0.3$  are nearly the same. Shifts of the ir modes with substitution of  $^{16}\text{O}$  with  $^{18}\text{O}$  are in accord with the expected role of oxygen in the various vibrational modes. The PA spectra of  $\text{YBa}_2\text{Cu}_3\text{A}\text{O}_{6+x}$  for pumping with 2.71-eV light across the band gap reveals the presence of a photoinduced electronic absorption band that varies with increasing oxygen content from a broad and nearly featureless peak at  $1300\text{ cm}^{-1}$  for  $x=0.0$ , to photoinduced transitions at 750, 950, 1100, and  $1300\text{ cm}^{-1}$  for  $x=0.13$  and  $0.20$ , and to a stronger PA peak centered at  $950\text{ cm}^{-1}$  with a shoulder at  $750\text{ cm}^{-1}$  for  $x=0.3$ . There are corresponding changes in the PA ir spectra with increasing  $x$ , with, in particular, bleaching of ir modes associated with the tetragonal  $x=0$  lattice and enhancement of ir modes associated with the orthorhombic  $x=1.0$  lattice. Based on our results and those from the following paper (Leng *et al.*), we propose a model for the formation of positively and negatively charged defects,  $D^+$  and  $D^-$ . We suggest that while the  $D^+$  defects reside on the  $\text{CuO}_2$  planes, the  $D^-$  defects consist of electrons initially in the conduction band for  $x=0.0$ . With increasing oxygen content, the electrons are trapped in  $\text{CuO}$  chains of increasing length and form localized  $D^-$  defects.

### I. INTRODUCTION

The infrared properties of the  $\text{YBa}_2\text{Cu}_3\text{O}_{6+x}$  system have been the subject of many studies. Numerous investigations on single crystals and thin films with the electric field polarized parallel to the  $\text{CuO}_2$  planes for  $x=1.0$  confirm that the phonon modes with displacements within the  $a$ - $b$  plane are almost screened by the free carriers.<sup>1,2</sup> The symmetry analysis of the lattice vibrations in semiconducting  $\text{YBa}_2\text{Cu}_3\text{O}_{6.0}$  is rather similar to that of metallic  $\text{YBa}_2\text{Cu}_3\text{O}_7$ , though the in-plane phonon modes are not screened and the vibrations with displacement along the  $a$  and  $b$  axis become degenerate with  $E_u$  symmetry. Previous measurements<sup>3,4</sup> of the far-infrared reflectance spectra of  $\text{YBa}_2\text{Cu}_3\text{O}_{6.0}$  have observed the five allowed  $A_{2u}$  modes and five of the six allowed  $E_u$  modes. Other measurements<sup>5</sup> report the observation of nine ir modes in the absorption spectra of semiconducting  $\text{YBa}_2\text{Cu}_3\text{O}_{6+x}$  ( $x \leq 0.5$ ). The existence of photoinduced charges and their properties have been studied through photoexcitation spectroscopy.<sup>6-11</sup> Previous experiments<sup>7,8,10</sup> reported photoinduced infrared-active vibrational (IRAV) modes and an associated electronic transition for semiconducting  $\text{YBa}_2\text{Cu}_3\text{O}_{6+x}$  with  $x=0.25$ ,

0.15–0.21, and 0.30, respectively, which indicated localized photoinduced charge carriers. The sites of these photoinduced defects were not identified.

In this paper we report our results of infrared- and photoinduced-absorption (PA) studies of  $\text{YBa}_2\text{Cu}_3\text{A}\text{O}_{6+x}$ , for  $A=16$  and  $18$  and for  $0 \leq x \leq 0.3$ , in the energy range  $80$ – $5000\text{ cm}^{-1}$ . We observed 10 of the 11 allowed infrared active modes in  $\text{YBa}_2\text{Cu}_3\text{O}_{6.3}$ , in agreement with previous reports.<sup>3,4</sup> We observed *all* 11 ir-active modes in  $\text{YBa}_2\text{Cu}_3\text{O}_{6.0}$ . The 11th mode (the 6th  $E_u$  mode) only appears at low temperature. The photoinduced absorption data are reported for samples of  $0 \leq x \leq 0.3$  and compared with earlier data obtained for a more limited composition region. The photoinduced spectra show a feature whose peak position and intensity is sensitive to composition, varying from broad and nearly featureless with a weak maximum at  $\sim 1300\text{ cm}^{-1}$  for  $x=0$  to photoinduced transitions at 750, 950, 1100, and  $1300\text{ cm}^{-1}$  for  $x=0.13$  and  $0.20$ , and to a stronger PA peak centered at  $950\text{ cm}^{-1}$ , with a shoulder at  $750\text{ cm}^{-1}$  for  $x=0.3$ . The photoinduced IRAV modes show variations with  $x$  as well, with increased absorption of orthorhombic modes and bleaching of tetragonal modes. When  $^{18}\text{O}$  is substituted for  $^{16}\text{O}$  in  $\text{YBa}_2\text{Cu}_3\text{O}_{6.3}$ , the ir-

absorption modes and photoinduced IRAV modes shift to lower energy, as expected. Based on these data and those from a companion paper,<sup>12</sup> we propose that upon photoexcitation positively charged defects  $D^+$  and negatively charged defects  $D^-$  form. We suggest that the  $D^+$  defects reside on the  $\text{CuO}_2$  planes and that the  $D^-$  defects consist of electrons initially in the conduction band for  $x=0$ , but with increasing  $x$  the electrons are trapped in  $\text{CuO}$  chains of increasing length, forming localized  $D^-$  defects.

In the next section of this paper we describe the experimental techniques used in this study, while in Sec. III we present experimental results for both direct- and photoinduced-absorption experiments. The data are discussed and a model proposed in Sec. IV. A summary of our work is presented in the final section.

## II. EXPERIMENTAL TECHNIQUES

Powder samples of  $\text{YBa}_2\text{Cu}_3\text{A}^{4}\text{O}_{6+x}$  ( $A=16$  and  $18$ ,  $0 \leq x \leq 0.3$ ) were prepared using previously described methods.<sup>3</sup> For the direct- and photoinduced-absorption measurements in the infrared, the powder samples ( $\sim 0.5$  wt %) were mixed with either  $\text{CsI}$  powder for use in the range  $180$ – $5000$   $\text{cm}^{-1}$  or with paraffin for the range  $20$ – $250$   $\text{cm}^{-1}$ . The sample-host mixture was then pressed under vacuum into uniform, partly transparent pellets. All sample handling was performed in an inert environment. Infrared measurements in the range  $20$ – $5000$   $\text{cm}^{-1}$  were made with a Nicolet 60SX Fourier transform infrared spectrometer. Far-ir measurements utilized a Ge bolometer, and for the mid-infrared, a MCT detector was used. The resolution in the far-ir was set to  $2$   $\text{cm}^{-1}$ , with spectra in the mid-ir measured at  $4$ - $\text{cm}^{-1}$  resolution. For temperature control, samples were attached to the end of a continuous-flow liquid-helium cryostat.

For the photoinduced-absorption measurements, the sample was optically pumped by an argon-ion laser at  $2.71$  eV ( $458$  nm) with intensities at the sample in the range  $40$ – $100$   $\text{mW}/\text{cm}^2$ . Spectra were recorded while alternately blocking and unblocking the laser, signal averaging until the desired signal-to-noise ratio was ob-

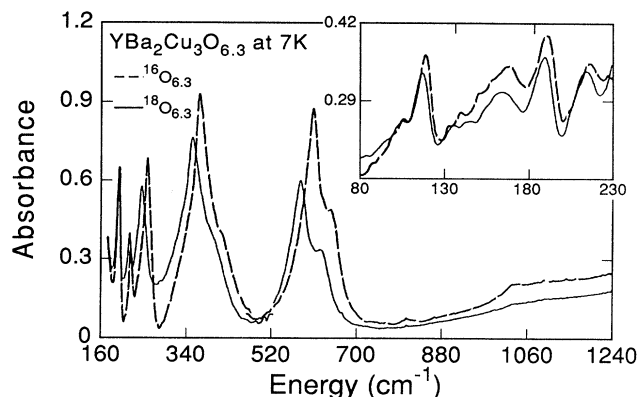


FIG. 1. Infrared-absorption spectra of  $\text{YBa}_2\text{Cu}_3\text{A}^4\text{O}_{6.3}$  in  $\text{CsI}$  (inset: in paraffin) at  $7$  K for  $A=16$  (dashed curve) and  $A=18$  (solid curve).

tained. The fractional change in the transmission of the sample,  $-\Delta T/T$ , was determined from the difference in absorption with the pump beam *off* and the pump beam *on* the sample.

## III. EXPERIMENTAL RESULTS

### A. Infrared-absorption spectra

The infrared-absorption spectra of  $\text{YBa}_2\text{Cu}_3\text{A}^4\text{O}_{6.3}$  ( $A=16,18$ ) in  $\text{CsI}$  and in paraffin at  $7$  K are shown in Fig. 1. We observe 10 of 11 allowed infrared active modes (listed in Table I), which are in close agreement with reflection spectra.<sup>3,4</sup> The five strongest modes ( $119$ ,  $194$ ,  $253$ ,  $364$ , and  $608$   $\text{cm}^{-1}$ ) all correspond to  $E_u$  vibrations, which are perpendicular to the  $c$  axis. The other five modes ( $107$ ,  $169$ ,  $219$ ,  $414$ , and  $644$   $\text{cm}^{-1}$ ) correspond to  $A_{2u}$  vibrations, which are parallel to the  $c$  axis.<sup>3</sup> The mode at  $414$   $\text{cm}^{-1}$  is weak and only appears at low temperature because of the phonon lifetime increasing with decreasing temperature, so that the phonon structures become more pronounced at low temperature. The pres-

TABLE I. Phonon energies (in  $\text{cm}^{-1}$ ) for  $\text{YBa}_2\text{Cu}_3\text{A}^4\text{O}_{6.3}$  ( $A=16$  and  $18$ ) at  $7$  and  $296$  K and for  $\text{YBa}_2\text{Cu}_3\text{A}^{16}\text{O}_{6.0}$  at  $27$  and  $296$  K. The symmetry identifications are from Ref. 3.

Symmetry	$\text{YBa}_2\text{Cu}_3\text{A}^{16}\text{O}_{6.3}$		$\text{YBa}_2\text{Cu}_3\text{A}^{18}\text{O}_{6.3}$		$\text{YBa}_2\text{Cu}_3\text{A}^{16}\text{O}_{6.0}$	
	7 K	296 K	7 K	296 K	27 K	296 K
$A_{2u}$	107	107	107	107	110	109
$E_u$	119	119	118	118	120	120
$A_{2u}$	169	168	165	164	168	167
$E_u$	194	191	193	190	193	190
$A_{2u}$	219	217	217	214	218	216
$E_u$	253	251	242	239	251	250
$E_u$					320sh <sup>a</sup>	
$E_u$	364	363	350	349	368	364
$A_{2u}$	414sh <sup>a</sup>		400sh <sup>a</sup>		403sh <sup>a</sup>	
$E_u$	608	589	581	565	604	588
$A_{2u}$	644	635	623	618	641	639

<sup>a</sup>sh = shoulder.

ence of these features is in agreement with previously reported reflection spectra.<sup>3,4</sup>

In Table I we list the vibrational modes observed when  $^{18}\text{O}$  is substituted for  $^{16}\text{O}$ , and we note that the isotopic shift agrees well with data reported by Crawford *et al.*<sup>3</sup> for  $\text{YBa}_2\text{Cu}_3\text{O}_{6.0}$ . Modes at 107, 119, 194, and 219  $\text{cm}^{-1}$  exhibit the smallest  $^{18}\text{O}$  shift ( $\leq 1\%$ ) and are attributed<sup>3</sup> to vibrations of the Ba and Y atoms. These modes are nearly unaffected by exchange of  $^{18}\text{O}$  for  $^{16}\text{O}$ . The other six modes at 169, 253, 364, 414, 608, and 644  $\text{cm}^{-1}$  exhibit the largest  $^{18}\text{O}$  shift ( $\geq 2\%$ ) and have been assigned<sup>3</sup> to Cu—O vibrations. The magnitude of the isotope shifts for the various modes is essentially unchanged as oxygen content increases from  $x=0$  to 0.3.

The infrared-absorption spectra of  $\text{YBa}_2\text{Cu}_3\text{O}_{6.0}$  in CsI and in paraffin at 27 and 300 K are shown in Fig. 2. We observe all 11 allowed infrared-active modes. The appearance of the absorption spectra is nearly the same as for  $\text{YBa}_2\text{Cu}_3\text{O}_{6.3}$  except for a weak shoulder at 320  $\text{cm}^{-1}$ . The modes at 403  $\text{cm}^{-1}$  (corresponding to the mode at 414  $\text{cm}^{-1}$  in  $\text{YBa}_2\text{Cu}_3\text{O}_{6.3}$ ) and at 320  $\text{cm}^{-1}$  are weak shoulders and only appear at low temperature. The mode at 320  $\text{cm}^{-1}$  is identified as the previously missed 11th  $E_u$  mode. The phonon lines exhibit a slight increase of their frequencies and intensities at low temperature (as also occurs for  $\text{YBa}_2\text{Cu}_3\text{O}_{6.3}$ ) except for the mode at 120  $\text{cm}^{-1}$ , which has a decrease of intensity at low temperature. In Table I we list the ir modes of  $\text{YBa}_2\text{Cu}_3\text{O}_{6.0}$  for comparison to those observed in  $\text{YBa}_2\text{Cu}_3\text{O}_{6.3}$ .

### B. Photoinduced-infrared-absorption spectra

Photoinduced-absorption (PA) spectra were measured for  $\text{YBa}_2\text{Cu}_3\text{O}_{6+x}$  with  $x=0.0, 0.13, 0.20,$  and  $0.30$ . The data in the range of 500–5000  $\text{cm}^{-1}$  (Figs. 3–6) show composition-dependent behavior, with a corresponding composition dependence of the photoinduced IRAV modes observed for  $x=0.0$  and  $0.3$  in the range 180–750  $\text{cm}^{-1}$ , shown in Figs. 7 and 8. The variation of these photoinduced IRAV modes with oxygen isotope for  $x=0.3$  is shown in Fig. 8.

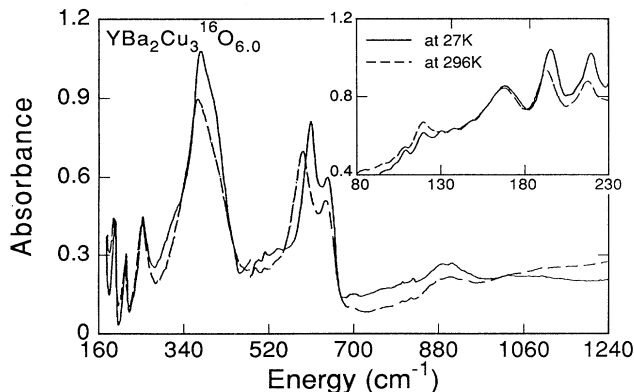


FIG. 2. Infrared-absorption spectra of  $\text{YBa}_2\text{Cu}_3\text{O}_{6.0}$  in CsI (inset: in paraffin) at 27 K (solid curve) and 295 K (dashed curve).

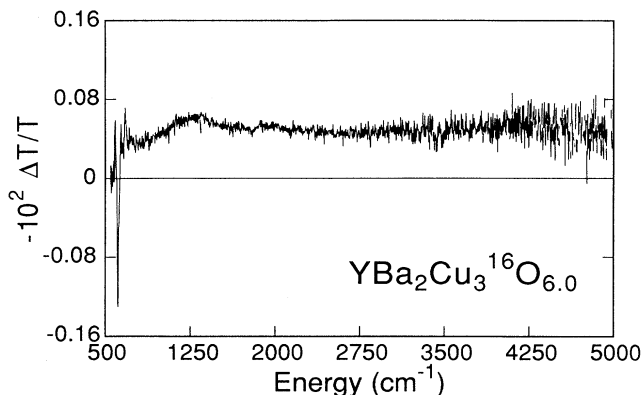


FIG. 3. Photoinduced-infrared-absorption spectrum of  $\text{YBa}_2\text{Cu}_3^{16}\text{O}_{6.0}$  in CsI at 27 K in the range of 500–5000  $\text{cm}^{-1}$ . The sample was pumped at 2.71 eV with intensity at the samples of 50  $\text{mW}/\text{cm}^2$ . See Fig. 7 for details of photoinduced vibrational structure.

The PA spectrum of  $\text{YBa}_2\text{Cu}_3\text{O}_{6.3}$ , shown in Fig. 6, is very similar to that reported earlier,<sup>7,9,10</sup> including the shape of the PA peak whose maximum is at  $\sim 950$   $\text{cm}^{-1}$ . A review of Figs. 3–6 reveals a systematic trend in the shape and peak position for this PA feature. For  $x=0.0$  (Fig. 3), this feature is broad with a weak maximum at  $\sim 1300$   $\text{cm}^{-1}$ . The PA signal does not return to zero even at energies as high as 5000  $\text{cm}^{-1}$ . Photoinduced near-ir and visible studies, in fact, show additional photoinduced absorption to energies higher than 1 eV.<sup>10,12</sup> For  $x=0.13$  (Fig. 4), the PA peak becomes more pronounced with “plateaus” at  $\sim 750$  and  $950$   $\text{cm}^{-1}$ , and a maximum at 1100  $\text{cm}^{-1}$ . With increasing  $x$ , for example,  $x=0.20$  (Fig. 5), “plateaus” are observed in the PA spectrum at  $\sim 750, 950, 1100,$  and  $1300$   $\text{cm}^{-1}$ . Finally, for  $x=0.3$  (Fig. 6), the PA spectrum has a well-defined peak at  $\sim 950$   $\text{cm}^{-1}$ , with a shoulder at 750  $\text{cm}^{-1}$ , while the

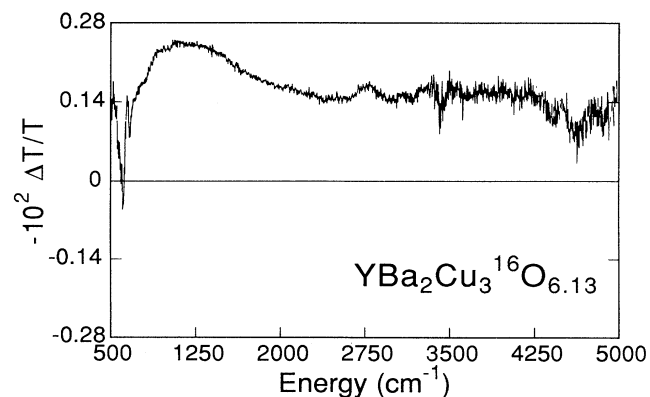


FIG. 4. Photoinduced-infrared-absorption spectrum of  $\text{YBa}_2\text{Cu}_3^{16}\text{O}_{6.13}$  in CsI at 25 K in the range of 500–5000  $\text{cm}^{-1}$ . The sample was pumped at 2.71 eV with intensity at the sample of 40  $\text{mW}/\text{cm}^2$ .

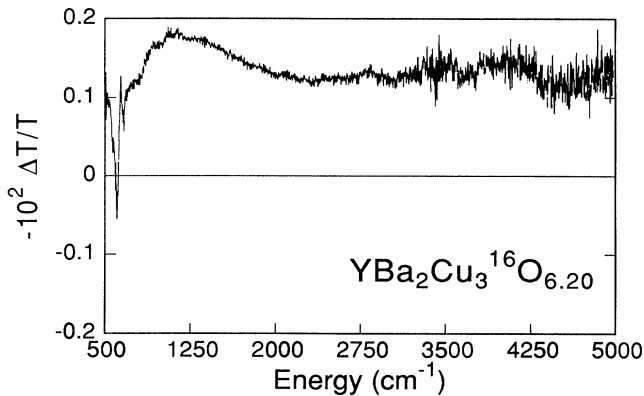


FIG. 5. Photoinduced-infrared-absorption spectrum of  $\text{YBa}_2\text{Cu}_3^{16}\text{O}_{6.20}$  in CsI at 25 K in the range of 500–5000  $\text{cm}^{-1}$ . The sample was pumped at 2.71 eV with intensity at the samples of 40  $\text{mW}/\text{cm}^2$ .

higher-energy PA signal is reduced with respect to the peak value.

The photoinduced infrared vibrational spectra of  $\text{YBa}_2\text{Cu}_3^A\text{O}_{6.3}$  for  $A=16$  and 18 in CsI at 7 K in the range 180–750  $\text{cm}^{-1}$  are shown in Fig. 8. We observe seven photoinduced-absorption modes and four photoinduced-bleaching (PB) modes. The photoinduced-absorption spectrum of  $\text{YBa}_2\text{Cu}_3^{18}\text{O}_{6.3}$  (Fig. 8) shows that all the photoinduced-absorption and -bleaching modes shifted to lower energy. The ratios of the PA and PB modes for the two isotopes show good agreement with the direct absorption results discussed in the previous section.

Attempts to extend the photoinduced measurements below 180  $\text{cm}^{-1}$  necessitated the use of a sample/paraffin configuration, in addition to polyethylene windows on the helium cryostat. Both of these changes increased the noise substantially in our measurements. Despite this,

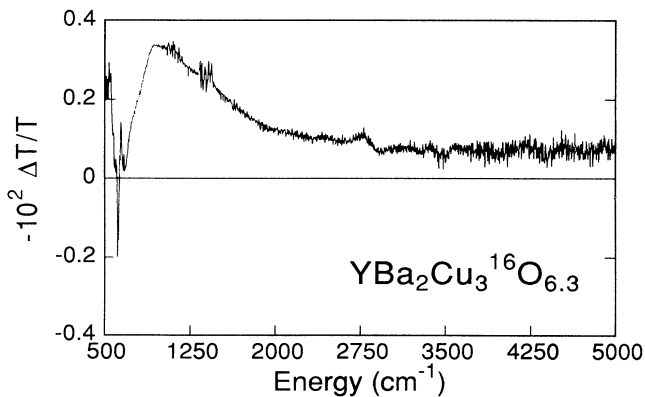


FIG. 6. Photoinduced-infrared-absorption spectrum of  $\text{YBa}_2\text{Cu}_3^{16}\text{O}_{6.3}$  in CsI at 7 K in the range of 500–5000  $\text{cm}^{-1}$ . The sample was pumped at 2.71 eV with intensity at the samples of 50–100  $\text{mW}/\text{cm}^2$ . See Fig. 8 for details of photoinduced vibrational structure.

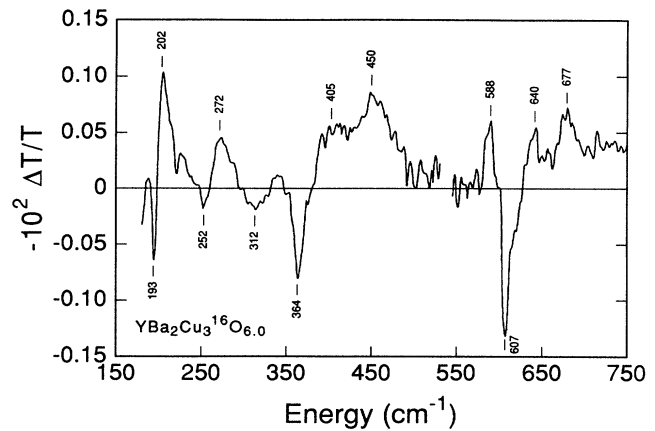


FIG. 7. Photoinduced-infrared-absorption spectrum of  $\text{YBa}_2\text{Cu}_3^{16}\text{O}_{6.0}$  in CsI at 27 K in the range of 180–750  $\text{cm}^{-1}$ . The sample was pumped at 2.71 eV with intensity at the samples of 50  $\text{mW}/\text{cm}^2$ . Peak positions are indicated in  $\text{cm}^{-1}$ .

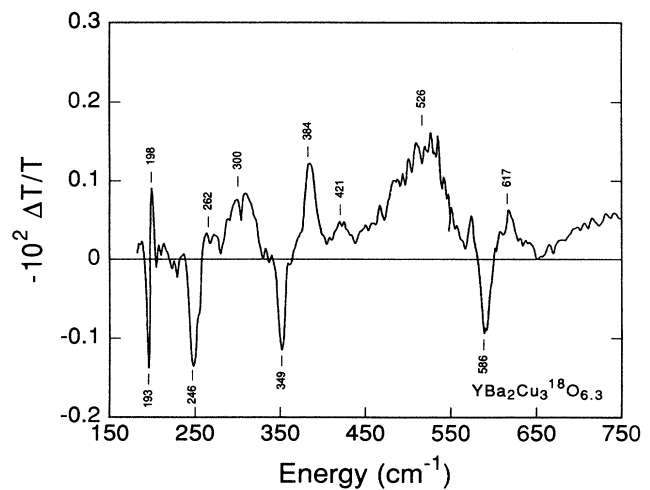
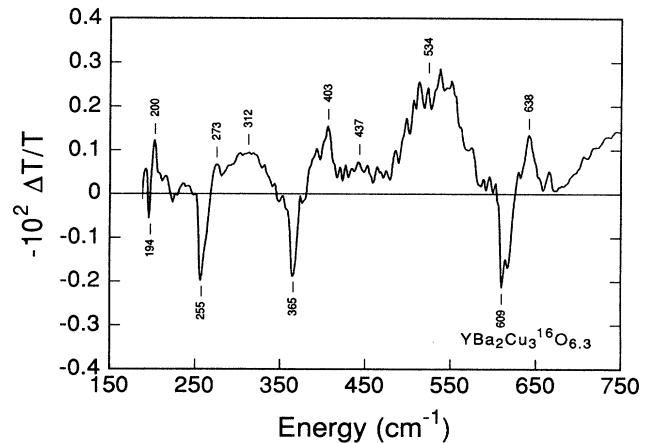


FIG. 8. Photoinduced-infrared-absorption spectrum of  $\text{YBa}_2\text{Cu}_3^A\text{O}_{6.3}$  for  $A=16$  (top) and  $A=18$  (bottom). Both experiments were for samples in CsI at 7 K in the range 180–750  $\text{cm}^{-1}$ . Both samples were pumped at 2.71 eV with intensity at the sample of 50–100  $\text{mW}/\text{cm}^2$ . Peak positions are indicated in  $\text{cm}^{-1}$ .

TABLE II. Assignment of photoinduced-absorption and -bleaching modes for  $\text{YBa}_2\text{Cu}_3\text{O}_{6.3}$  at 7 K and  $\text{YBa}_2\text{Cu}_3\text{O}_{6.0}$  at 27 K. Phonon energies are in  $\text{cm}^{-1}$ .

$\text{YBa}_2\text{Cu}_3\text{O}_{6.3}$	Assignment	$\text{YBa}_2\text{Cu}_3\text{O}_{6.0}$	Assignment
200 (PA)	194 ir in $O_7$	202 (PA)	194 ir in $O_7$
273 (PA)	276 ir in $O_7$	272 (PA)	276 ir in $O_7$
312 (PA)	312 ir in $O_7$		
		337 (PA)	343 Raman in $O_6$
403 (PA)	420 Raman in $\text{BaCuO}_2$	405 (PA)	420 Raman in $\text{BaCuO}_2$
437 (PA)	435 Raman in $O_7$		
534 (PA)	502 Raman in $O_7$	450 (PA)	456 Raman in $O_6$
	572 Raman in $O_7$		475 Raman in $O_6$
		588 (PA)	572 ir in $O_7$
638 (PA)	641 Raman in $\text{BaCuO}_2$	640 (PA)	641 Raman in $\text{BaCuO}_2$
		677 (PA)	
194 (PB)	194 ir $E_u$ mode in $O_{6.3}$	193 (PB)	193 ir $E_u$ mode in $O_{6.0}$
255 (PB)	253 ir $E_u$ mode in $O_{6.3}$	252 (PB)	251 ir $E_u$ mode in $O_{6.0}$
		312 (PB)	302 ir $E_u$ mode in $O_{6.0}$
365 (PB)	364 ir $E_u$ mode in $O_{6.3}$	364 (PB)	368 ir $E_u$ mode in $O_{6.0}$
609 (PB)	608 ir $E_u$ mode in $O_{6.3}$	607 (PB)	604 ir $E_u$ mode in $O_{6.0}$

there is agreement between the ir spectra obtained using the paraffin configuration and those using the CsI window and CsI matrix at energies above  $180 \text{ cm}^{-1}$ .

The photoinduced-absorption spectrum of  $\text{YBa}_2\text{Cu}_3\text{O}_{6.0}$  in the range  $180\text{--}750 \text{ cm}^{-1}$  at 27 K is shown in Fig. 7. We observed eight vibrational PA modes and five vibrational PB modes in addition to the weak, broad band peaked at  $\sim 1300 \text{ cm}^{-1}$ . Table II lists all photoinduced-absorption and -bleaching vibrational modes of  $\text{YBa}_2\text{Cu}_3\text{O}_{6.0}$ , together with data of  $\text{YBa}_2\text{Cu}_3\text{O}_{6.3}$ . The photoinduced IRAV modes for the two materials are nearly the same, although there are some differences. The photoexcitation spectrum of  $\text{YBa}_2\text{Cu}_3\text{O}_{6.0}$  has a new PB mode at  $312 \text{ cm}^{-1}$  instead of a PA mode as observed in  $\text{YBa}_2\text{Cu}_3\text{O}_{6.3}$  and has two PA modes centered at 450 and  $588 \text{ cm}^{-1}$  instead of a strong, broad mode at  $534 \text{ cm}^{-1}$  in  $\text{YBa}_2\text{Cu}_3\text{O}_{6.3}$ . We discuss the assignments in detail in the next section.

Because of the appearance of some of the photoinduced IRAV modes as derivativelike features, extensive measurements were made to determine if any features were due to possible heating of the sample while it was exposed to the intense pump beam. Heating-induced absorption data were determined by computing  $-\Delta T/T$  from the difference in spectra obtained at 7 K and at slightly higher temperatures, e.g., 15 or 30 K. None of the features that we report in our photoinduced experiments were reproducible in the heating-induced experiments, and so we take the photoinduced spectral features to be real. In addition, spectra obtained at different laser intensities varied sublinearly with laser power, supporting this conclusion.

#### IV. DISCUSSION

##### A. Infrared-absorption spectra

According to theoretical analysis,<sup>5,13</sup> there are five  $A_{2u}$  modes that are parallel to the  $c$  axis and six  $E_u$  modes

that are perpendicular to the  $c$  axis in  $\text{YBa}_2\text{Cu}_3\text{O}_{6.0}$ . Detailed infrared-reflection studies of  $\text{YBa}_2\text{Cu}_3\text{O}_{6.0}$  have been reported. Crawford *et al.*<sup>3</sup> compared near-normal-incidence Cu-O plane reflectivity of a single crystal with the data of ceramic samples in order to extract the  $A_{2u}$  modes. Bauer *et al.*<sup>4</sup> have reported an ir study on an oriented crystal block with incident field parallel and perpendicular to the  $c$  axis. Both investigations reported all five  $A_{2u}$  modes and five of the six allowed  $E_u$  modes. The 11th mode (an in-plane  $E_u$  mode) is absent in the previous reports on ceramics,<sup>13,14</sup> single crystals,<sup>3</sup> and highly oriented multicrystalline blocks<sup>4</sup> of  $\text{YBa}_2\text{Cu}_3\text{O}_{6.0}$ .

We observed 10 ir modes (5  $E_u$  and 5  $A_{2u}$ ) at low temperature for  $\text{YBa}_2\text{Cu}_3\text{O}_{6.3}$ , which are in good agreement with reflection experiments.<sup>3,4</sup> We observed 11 modes (6  $E_u$  and 5  $A_{2u}$ ) at low temperature for  $\text{YBa}_2\text{Cu}_3\text{O}_{6.0}$ . The 11th mode at  $320 \text{ cm}^{-1}$  is quite weak and disagrees with the theoretical prediction<sup>13</sup> that the 11th mode is near  $55\text{--}62 \text{ cm}^{-1}$ . We assign this mode at  $320 \text{ cm}^{-1}$  to the previously missing  $E_u$  mode for the following reasons: (1) Comparing the absorption spectrum at 27 K with the spectrum at 300 K, one finds that the weak shoulder at  $\sim 320 \text{ cm}^{-1}$  appears only at 27 K. (2) A comparison of the absorption spectrum of  $\text{YBa}_2\text{Cu}_3\text{O}_{6.3}$  with the spectrum of  $\text{YBa}_2\text{Cu}_3\text{O}_{6.0}$  reveals that they are nearly identical, though the spectrum of  $\text{YBa}_2\text{Cu}_3\text{O}_{6.0}$  has more absorption in the range between the two absorption peaks ( $E_u$  modes at 251 and  $368 \text{ cm}^{-1}$ ). (3) All photoinduced-bleaching modes in  $\text{YBa}_2\text{Cu}_3\text{O}_{6.0}$  and  $\text{YBa}_2\text{Cu}_3\text{O}_{6.3}$  correspond directly to the  $E_u$  modes that appear in the direct-absorption spectra. By comparison, the bleaching mode at  $312 \text{ cm}^{-1}$  seen for  $\text{YBa}_2\text{Cu}_3\text{O}_{6.0}$  corresponds to one  $E_u$  mode. This bleaching mode at  $312 \text{ cm}^{-1}$  is evidence for the existence of the sixth  $E_u$  mode. Usually, missing modes either have very small oscillator strength or are located near in energy to another mode, thereby making it difficult to distinguish. For  $\text{YBa}_2\text{Cu}_3\text{O}_{6.0}$ , the  $E_u$  mode at

TABLE III. Comparison of calculated and measured ir modes of  $\text{YBa}_2\text{Cu}_3\text{O}_{6.0}$ .

Calculation ( $\text{cm}^{-1}$ )			Experiment ( $\text{cm}^{-1}$ )		
Symmetry	$\omega_{\text{TO}}$ ( $\omega_{\text{LO}}$ ) <sup>a</sup>	$\omega^b$	Reflection $\omega_{\text{TO}}$ ( $\omega_{\text{LO}}$ ) <sup>c</sup>	Absorption $\omega^d$	Reflection $\omega_{\text{TO}}$ ( $\omega_{\text{LO}}$ ) <sup>e</sup>
$A_{2u}$	116 (119)	73	107 (109)	110	105 (110)
$A_{2u}$	153 (163)	181	154 (180)	168	146 (180)
$A_{2u}$	189 (203)	235	217 (220)	218	215 (222)
$A_{2u}$	390 (455)	371	442 (458)	400	367 (470)
$A_{2u}$	540 (543)	606	648 (663)	641	645 (664)
$E_u$	55 (62)	88	118 (124)	120	116 (125)
$E_u$	105 (106)	125	190 (195)	193	188 (199)
$E_u$	214 (243)	187	248 (264)	251	246 (266)
$E_u$	276 (318)	400		320	
$E_u$	355 (414)	546	352 (418)	368	351 (420)
$E_u$	502 (507)	643	589 (628)	603	595 (637)

<sup>a</sup>Reference 13.<sup>b</sup>Reference 15.<sup>c</sup>Reference 3.<sup>d</sup>Our data.<sup>e</sup>Reference 4.

$320 \text{ cm}^{-1}$  is located near the  $E_u$  mode at  $368 \text{ cm}^{-1}$  and overlaps with it, so that we only observe a shoulder.

We comment here on the comparison of our results to lattice-dynamics calculations<sup>13,15</sup> for  $\text{YBa}_2\text{Cu}_3\text{O}_{6.0}$ . These calculations appear to agree more closely with Raman measurements than with ir measurements. Our data are in good agreement with reflection measurements by Crawford *et al.*<sup>3</sup> and Bauer *et al.*<sup>4</sup> The 11th mode that we report disagrees with theoretical calculations, which predict that it is the lowest-lying phonon mode ( $60\text{--}90 \text{ cm}^{-1}$ ), although the other 10 modes are similar to the calculated frequencies. In general, ir-active modes can involve motion of every ion in the unit cell, whereas Raman-active modes are restricted by symmetry to involve motion of certain ions only.<sup>3</sup> Thus the Raman-active modes are simpler in form than ir-active modes and may account for the better agreement with predictions. Table III summarizes the predicted ir modes and compares them to experimental reflection and absorption results.

### B. Vibrational photoexcitation spectra

The PA spectra of  $\text{YBa}_2\text{Cu}_3\text{O}_{6.3}$  (Fig. 8) show five photoinduced-bleaching modes, eight photoinduced-absorption modes, and a broad electronic transition centered at  $\sim 1000 \text{ cm}^{-1}$ . All five bleaching modes correspond directly to the five  $E_u$  modes seen in direct absorption experiments, and five of eight photoinduced-absorption modes correspond to the ir modes of the orthorhombic phase  $\text{YBa}_2\text{Cu}_3\text{O}_7$ .<sup>3</sup> These results imply that the activity of the ir modes in the tetragonal phase of  $\text{YBa}_2\text{Cu}_3\text{O}_{6.3}$  is reduced, and some ir modes of  $\text{YBa}_2\text{Cu}_3\text{O}_7$  appear upon photoexcitation.

Three other photoinduced-absorption modes may be due to symmetry breaking that could cause formerly Raman modes to become ir active. The two PA modes at

403 and  $638 \text{ cm}^{-1}$  may be due to impurity phases of  $\text{BaCuO}_2$ . The Raman data of Rosen *et al.*<sup>16</sup> reveal modes at 420 and  $641 \text{ cm}^{-1}$  due to the presence of  $\text{BaCuO}_2$  in  $\text{YBa}_2\text{Cu}_3\text{O}_7$ . The amount of impurity phases in the parent material appears to be quite small from the lack of ir signal, but the presence of PA modes may indicate that the photoinduced-absorption experiment is a very sensitive probe of the impurity phase. The very weak PA mode at  $\sim 437 \text{ cm}^{-1}$  has been previously attributed to a Raman mode of the tetragonal phase.<sup>7,9</sup> The PA mode at  $534 \text{ cm}^{-1}$  has also been previously assigned to a Raman mode, although our data indicate that, while there may be some contribution from this source, a contribution from the  $572\text{-cm}^{-1}$  ir mode of  $\text{YBa}_2\text{Cu}_3\text{O}_7$  may be the dominant feature. The splitting of this photoinduced-absorption peak into two peaks at 450 and  $588 \text{ cm}^{-1}$  in  $\text{YBa}_2\text{Cu}_3\text{O}_{6.0}$  supports this assignment.

For  $\text{YBa}_2\text{Cu}_3\text{O}_{6.0}$ , the photoinduced infrared-active vibrations observed include five bleaching modes and eight photoinduced-absorption modes. The PA spectra of  $\text{YBa}_2\text{Cu}_3\text{O}_{6.3}$  and  $\text{YBa}_2\text{Cu}_3\text{O}_{6.0}$  have many similarities: The bleaching modes correspond to  $E_u$  ir modes, some PA modes correspond to ir modes of  $\text{YBa}_2\text{Cu}_3\text{O}_7$ , and some PA modes correspond to Raman modes. In addition, there are some changes in individual modes. As noted above, in the PA spectrum of  $\text{YBa}_2\text{Cu}_3\text{O}_{6.0}$  there is one additional bleaching mode at  $312 \text{ cm}^{-1}$  because of the sixth  $E_u$  mode observable in  $\text{YBa}_2\text{Cu}_3\text{O}_{6.0}$ . We report also a weak PA vibrational mode at  $337 \text{ cm}^{-1}$  for  $x=0$ ; a weak PA vibrational mode is observed at  $437 \text{ cm}^{-1}$  for  $x=0.3$ . Instead of a strong broad PA mode observed at  $534 \text{ cm}^{-1}$  for  $\text{YBa}_2\text{Cu}_3\text{O}_{6.3}$ , there are two new PA modes at 450 and  $588 \text{ cm}^{-1}$  in  $\text{YBa}_2\text{Cu}_3\text{O}_{6.0}$ . Thomsen *et al.*<sup>13,17</sup> report the variation of Raman modes for  $\text{YBa}_2\text{Cu}_3\text{O}_{6+x}$  with oxygen content. They show four Raman modes at 154, 334, 438, and  $502 \text{ cm}^{-1}$  for

YBa<sub>2</sub>Cu<sub>3</sub>O<sub>7</sub> and at 144, 343, 456, and 475 cm<sup>-1</sup> for YBa<sub>2</sub>Cu<sub>3</sub>O<sub>6.0</sub>. As the oxygen content is decreased, the two modes at 502 and 438 cm<sup>-1</sup> shift toward each other, while the mode at 334 cm<sup>-1</sup> shifts to higher frequency with an increase in intensity (the intensity of 343 cm<sup>-1</sup> in YBa<sub>2</sub>Cu<sub>3</sub>O<sub>6.0</sub> is about 3 times its value in YBa<sub>2</sub>Cu<sub>3</sub>O<sub>6.3</sub>). Comparing our data for the  $x=0$  material to these Raman results, we assign the PA mode at 337 cm<sup>-1</sup> as corresponding to the Raman mode at 343 cm<sup>-1</sup> of YBa<sub>2</sub>Cu<sub>3</sub>O<sub>6.0</sub>, the PA mode at 450 cm<sup>-1</sup> as corresponding to the Raman modes at 456 and 475 cm<sup>-1</sup>, and the PA mode at 588 cm<sup>-1</sup> as corresponding to an ir mode of YBa<sub>2</sub>Cu<sub>3</sub>O<sub>7</sub>. The assignments of the PA and PB modes in YBa<sub>2</sub>Cu<sub>3</sub>O<sub>6.0</sub> and YBa<sub>2</sub>Cu<sub>3</sub>O<sub>6.3</sub> are listed in Table II. The origin of the 677-cm<sup>-1</sup> PA mode is not assigned here.

### C. Photoinduced electronic transition

The photoinduced electronic transition observed for YBa<sub>2</sub>Cu<sub>3</sub>O<sub>6+x</sub> varies systematically with  $x$  (Figs. 3–6). For  $x=0$ , the photoinduced-absorption spectrum has a weak maximum at  $\sim 1300$  cm<sup>-1</sup> and a broad absorption extending to above  $\sim 5000$  cm<sup>-1</sup>. The photoinduced absorption becomes more peaked with a “plateau” structure appearing as  $x$  increases to 0.13, 0.20, and higher. As noted in Sec. III B for  $x=0.3$ , the photoinduced absorption is more strongly peaked at 950 cm<sup>-1</sup>, with only a shoulder appearing at 750 cm<sup>-1</sup>. The intensity of the photoinduced absorption is smallest for  $x=0$ , intermediate for  $x=0.13$  and 0.20, and largest for  $x=0.3$ . An amplitude-mode analysis<sup>18</sup> is not presented because the photoinduced absorption does not decrease to zero at the higher energies in this experiment and there is no concomitant photoinduced bleaching observed in the range from 0 to 5000 cm<sup>-1</sup>.

### D. Proposed model

To explain the origin of the photoinduced-absorption spectra, we propose a model that describes the ground- and excited-state properties of YBa<sub>2</sub>Cu<sub>3</sub>O<sub>6+x</sub>. Based on electronic-structure calculations,<sup>19,20</sup> the two highest-lying valence bands are composed primarily of oxygen  $2p_{x,y}$  and copper  $d$  bonding orbitals in the CuO<sub>2</sub> planes. Similarly, the conduction band has been proposed<sup>19,20</sup> to be composed primarily of antibonding  $pd\sigma$  bands with a gap of approximately 2 eV between the valence and conduction bands. Absorption of a 2.71-eV photon in the photoexcitation experiment then leads to a hole in the valence band and an electron in the conduction band.

For YBa<sub>2</sub>Cu<sub>3</sub>O<sub>6.0</sub>, ignoring lattice relaxation, the hole would be mobile within the CuO<sub>2</sub> planes. The ability of this hole to move and screen the  $E_u$  modes, which are polarized parallel to the CuO<sub>2</sub> planes, may account for the photoinduced bleaching observed for each of the  $E_u$  modes in YBa<sub>2</sub>Cu<sub>3</sub>O<sub>6.0</sub> and YBa<sub>2</sub>Cu<sub>3</sub>O<sub>6.3</sub>. The accompanying paper by Leng *et al.*<sup>12</sup> reports the formation of two new photoinduced absorptions in the gap at 1.1 and 1.4 eV. These photoexcitations may be associated with a  $D^+$  polaronlike defect formed in the gap due to deforma-

tion of the CuO<sub>2</sub> planes.<sup>12</sup> The 1.1- and 1.4-eV absorptions then correspond to excitation to the defect level from the two highest-lying valence bands. It is noted that the actual polaron level may lie substantially closer to the valence-band edge as the 1.1- and 1.4-eV photoinduced absorptions include the effects of Coulomb repulsion for inserting a second charge into the polaron level.

Similarly, the photoexcited electron is expected to delocalize in the conduction band formed from the Cu  $4s$  states. This free carrier in the bottom of the conduction band may account for the presence of the broad photoinduced absorption observed in the  $x=0$  samples, which is present to a lesser extent in the samples with higher oxygen content.

With increasing oxygen content, starting from  $x=0$ , oxygen is added to the Cu layer, which eventually constitutes the CuO chain layer when  $x=1.0$ . For low  $x$ , short “moleculelike” segments of  $(\text{Cu}^{2+}\text{O}^{2-})_y\text{Cu}^{2+}$  are expected to form. The presence of the weak photoinduced-absorption maximum at 1300 cm<sup>-1</sup> for the  $x=0$  samples and the growth of new plateaus at 1100, 950, and 750 cm<sup>-1</sup> for increasing oxygen content lead to the speculation that these photoinduced absorptions are due to the formation of photoexcited anioniclike states in the molecular  $(\text{Cu}^{2+}\text{O}^{2-})_y\text{Cu}^{2+}$ . The distribution of lengths  $y$  of these units will depend upon the oxygen content  $x$  in the material. These units are expected to be traps for the photoexcited electrons, forming  $[(\text{Cu}^{2+}\text{O}^{2-})_y\text{Cu}^{2+}]^{-1}$ . The trapping of the photoexcited electron to form these anionic units, which are orthorhombic in symmetry, may lead to the enhancement of orthorhombic infrared modes, i.e., the increase in the ir vibrational absorptions observed in the photoexcitation spectra and the reduction of the photoinduced continuumlike absorption with increasing  $x$ . Intramolecular excitations within the anionic molecule (or excitation from the highest occupied orbital in the anionic molecule to the conduction band) may then constitute the photoinduced absorption observed with peaks at 1300, 1100, 950, and 750 cm<sup>-1</sup>. The discrete values of this photoinduced absorption are suggested to be related to the length of the molecule  $y$ , with longer molecules having lower excitation energies. The observed photoinduced-absorption peak then reflects the distribution of molecular lengths in the YBa<sub>2</sub>Cu<sub>3</sub>O<sub>6+x</sub> material.

To summarize, we propose a scheme in which the photoexcited hole forms a polaron that is mobile within the CuO<sub>2</sub> planes and screens the  $E_u$  vibrations, while the photoexcited electron introduces a continuum of photoinduced absorption as long as it remains in the conduction band. A trapping mechanism for the photoexcited electron involving  $(\text{Cu}^{2+}\text{O}^{2-})_y\text{Cu}^{2+}$  molecules is suggested for the photoexcited electrons. Photoinduced absorptions arising from these molecular units are suggested as the origin of the photoexcitations observed at 750–1300 cm<sup>-1</sup> and the photoinduced orthorhombic vibration modes.

## V. CONCLUSION

We have reported direct- and photoinduced-absorption spectra of semiconducting YBa<sub>2</sub>Cu<sub>3</sub>A<sub>4</sub>O<sub>6+x</sub> for  $A=16$

and 18 and for  $0 \leq x \leq 0.3$ . Our direct- and photoinduced-absorption measurements allow the identification of all 11 ir-active modes ( $5 A_{2u} + 6 E_u$ ) in  $\text{YBa}_2\text{Cu}_3\text{O}_{6.0}$ . The 11th mode ( $E_u$ ), which is missing in previous reports, is identified at  $\sim 320 \text{ cm}^{-1}$ .

The infrared photoexcitation spectroscopy identifies important photoexcited vibrational and electronic features that vary with the oxygen content  $x$ . The systematic bleaching of the  $E_u$  modes and photoinduced absorption of  $A_{2u}$  modes together with the variation of the photoinduced electronic transition energy with increasing

$x$  has led to the proposal of a model wherein the holes form mobile polarons within the  $\text{CuO}_2$  layers, screening the  $E_u$  vibrations, while the photoexcited electrons move within the conduction band or become trapped on segments of  $\text{CuO}$  chains.

#### ACKNOWLEDGMENTS

This work is supported in part by the Defense Advanced Research Projects Agency through a contract monitored by the U.S. Office of Naval Research.

\*Present address: Shanghai Institute of Technical Physics, Shanghai, People's Republic of China.

<sup>1</sup>G. A. Thomas, J. Orenstein, D. H. Rapkine, M. Capizzi, A. J. Mills, R. N. Bhatt, L. F. Schneemeyer, and J. V. Waszczak, *Phys. Rev. Lett.* **61**, 1313 (1988).

<sup>2</sup>R. T. Collins, Z. Schlesinger, F. Holtzberg, P. Chaudhari, and C. Feild, *Phys. Rev. B* **39**, 6571 (1989).

<sup>3</sup>M. K. Crawford, W. E. Farneth, E. M. McCarron III, and R. K. Bordia, *Phys. Rev. B* **38**, 11 382 (1988); M. K. Crawford, G. Burns, and F. Holtzberg, *Solid State Commun.* **70**, 557 (1989).

<sup>4</sup>M. Bauer, I. B. Ferreira, L. Genzel, M. Cardona, P. Murugaraj, and J. Maier, *Solid State Commun.* **72**, 551 (1989).

<sup>5</sup>G. Burns, F. H. Dacol, P. Freitas, T. S. Plaskett, and W. König, *Solid State Commun.* **64**, 471 (1987).

<sup>6</sup>J. M. Ginder, M. G. Roe, Y. Song, R. P. McCall, J. R. Gaines, E. Ehrenfreund, and A. J. Epstein, *Phys. Rev. B* **37**, 7506 (1988).

<sup>7</sup>C. Taliani, R. Zamboni, G. Ruani, F. C. Matacotta, and K. I. Pokhodnya, *Solid State Commun.* **66**, 487 (1988); C. Taliani, R. Zamboni, G. Ruani, A. J. Pal, F. C. Matacotta, Z. Vardeny, and X. Wea, in *High  $T_c$  Superconductors Electronic Structure*, edited by A. Bianconi and A. Marcelli (Pergamon, Oxford, 1989), p. 95.

<sup>8</sup>Y. H. Kim, A. J. Heeger, L. Acedo, G. Stucky, and F. Wudl, *Phys. Rev. B* **36**, 7252 (1987).

<sup>9</sup>Y. H. Kim, C. M. Foster, A. J. Heeger, S. Cox, and G. Stucky, *Phys. Rev. B* **38**, 6478 (1988).

<sup>10</sup>A. J. Epstein, J. M. Ginder, J. M. Leng, R. P. McCall, M. G. Roe, H. J. Ye, W. E. Farneth, E. M. McCarron III, and S. I. Shah, in *High  $T_c$  Superconductors Electronic Structure*, edited by A. Bianconi and A. Marcelli (Pergamon, Oxford, 1989), p. 87.

<sup>11</sup>C. M. Foster, A. J. Heeger, Y. H. Kim, G. Stucky, and N. Herron, *Synth. Met.* **33**, 171 (1989).

<sup>12</sup>J. M. Leng, J. M. Ginder, W. E. Farneth, S. I. Shah, and A. J. Epstein, following paper, *Phys. Rev. B* **43**, 10 582 (1991).

<sup>13</sup>C. Thomsen, M. Cardona, W. Kress, R. Liu, L. Genzel, M. Bauer, and E. Schön herr, *Solid State Commun.* **65**, 1139 (1988).

<sup>14</sup>G. Burns, F. H. Dacol, P. P. Freitas, W. König, and T. S. Plaskett, *Phys. Rev. B* **37**, 5171 (1988).

<sup>15</sup>F. E. Bates, *Phys. Rev. B* **39**, 322 (1989).

<sup>16</sup>H. J. Rosen, R. M. Macfarlane, E. M. Engler, V. Y. Lee, and R. D. Jacowitz, *Phys. Rev. B* **38**, 2460 (1988).

<sup>17</sup>C. Thomsen, R. Liu, M. Bauer, A. Wittlin, L. Genzel, M. Cardona, E. Schön herr, W. Bauhofer, and W. König, *Solid State Commun.* **65**, 55 (1988).

<sup>18</sup>E. Ehrenfreund, Z. Vardeny, O. Bratman, and B. Horowitz, *Phys. Rev. B* **36**, 1535 (1987).

<sup>19</sup>L. F. Mattheiss and D. R. Hamann, *Solid State Commun.* **63**, 395 (1987).

<sup>20</sup>S. Massidda, J. Yu, A. J. Freeman, and D. D. Koelling, *Phys. Lett. A* **122**, 198 (1987); J. Yu, S. Massidda, A. J. Freeman, and D. D. Koelling, *ibid.* **122**, 203 (1987).